







Publication Year	2021
Acceptance in OA @INAF	2023-09-13T12:18:18Z
Title	Icarus: a flat and fast prograde stellar stream in the Milky Way disk
Authors	RE FIORENTIN, Paola; SPAGNA, Alessandro; LATTANZI, Mario Gilberto; Cignoni, Michele
DOI	10.3847/2041-8213/abd53d
Handle	http://hdl.handle.net/20.500.12386/34384
Journal	THE ASTROPHYSICAL JOURNAL LETTERS
Number	907



Icarus: A Flat and Fast Prograde Stellar Stream in the Milky Way Disk

Paola Re Fiorentin¹ , Alessandro Spagna¹ , Mario G. Lattanzi^{1,2} , and Michele Cignoni^{3,4,5} 

¹ INAF - Osservatorio Astrofisico di Torino, Strada Osservatorio 20, I-10025 Pino Torinese (TO), Italy; paola.refiorentin@inaf.it

² Department of Physics, University of Torino, Via Giuria 1, I-10125 Torino, Italy

³ Department of Physics, University of Pisa, Largo Pontecorvo 3, I-56127 Pisa, Italy

⁴ INFN, Largo B. Pontecorvo 3, I-56127 Pisa, Italy

⁵ INAF - Osservatorio di Astrofisica e Scienza dello Spazio, Via Gobetti 93/3, I-40129 Bologna, Italy

Received 2020 October 17; revised 2020 December 15; accepted 2020 December 19; published 2021 January 20

Abstract

We explore the local volume of the Milky Way via chemical and kinematical measurements from high-quality astrometric and spectroscopic data recently released by the Gaia, APOGEE, and GALAH programs. We chemically select 1137 stars up to 2.5 kpc of the Sun and $[\text{Fe}/\text{H}] \leq -1.0$ dex, and find evidence of statistically significant substructures. Clustering analysis in velocity space classifies 163 objects into eight kinematical groups, whose origin is further investigated with high-resolution N -body numerical simulations of single merging events. The two retrograde groups appear associated with Gaia-Sausage-Enceladus (GSE), while the slightly prograde group could be connected to GSE or possibly Wukong. We find evidence of a new 44-member-strong prograde stream that we name Icarus; to our knowledge, Icarus is the fast-rotating stream closest to the Galactic disk to date ($\langle Z_{\text{max}} \rangle \lesssim 0.5$ kpc, $\langle V + V_{\text{LSR}} \rangle \simeq 231$ km s⁻¹). Its peculiar chemical ($\langle [\text{Fe}/\text{H}] \rangle \simeq -1.45$, $\langle [\text{Mg}/\text{Fe}] \rangle \simeq -0.02$) and dynamical (mean eccentricity $\simeq 0.11$) properties are consistent with the accretion of debris from a dwarf galaxy progenitor with a stellar mass of $\sim 10^9 M_{\odot}$ on an initial prograde low-inclination orbit, $\sim 10^{\circ}$. **The remaining prograde groups are either streams previously released by the same progenitor of Icarus (or Nyx), or remnants from different satellites accreted on initial orbits at higher inclination.**

Unified Astronomy Thesaurus concepts: Milky Way formation (1053); Milky Way stellar halo (1060); Milky Way dynamics (1051); Stellar abundances (1577)

1. Introduction

According to current formation models, galaxies like the Milky Way (MW) grow by mergers of smaller satellites over their lifetime. Simulations based on this cosmological paradigm show that tidal forces can distort or even disrupt low-mass systems orbiting a MW analog. This process rips out stars from the progenitors, leaving them as fossil debris with inhomogeneous distributions in the spheroidal (halo-like) component of the host (Johnston 1998; Bullock & Johnston 2005; Cooper et al. 2010; Fattahi et al. 2020).

Considerable structure is still present in the Galactic halo that does retain memory of its accretion history in the form of streams of stars (e.g., Ibata et al. 1994; Malhan et al. 2018; Naidu et al. 2020). Besides, in the vicinity of the Sun (within, say, 3 kpc), where strong phase-mixing takes place, merger debris can still be identified as kinematical coherent streams despite of being spatially undetectable (Helmi et al. 1999; Smith et al. 2009; Klement 2010; Re Fiorentin et al. 2015).

Recent studies confirmed that a massive dwarf galaxy, named Gaia-Sausage-Enceladus (GSE), merged with the MW ~ 10 Gyr ago (Belokurov et al. 2018; Helmi et al. 2018; Di Matteo et al. 2019; Gallart et al. 2019).

More kinematical and chemical substructures with retrograde motions have been found among MW halo stars, i.e., Sequoia by Myeong et al. (2019), Thamnos by Koppelman et al. (2019b), and dynamically tagged groups (DTGs) of Yuan et al. (2020). Conversely, the prograde part of the halo has been little explored. Likely, the reason is the traditional kinematical selection criteria that reject as halo stars objects with

$\|v - v_{\text{LSR}}\| < v_{\text{lim}}$, where $v_{\text{lim}} = 180 \div 230$ km s⁻¹ (Nissen & Schuster 2010; Koppelman et al. 2019b).

The detection of accreted stars in the Galactic disk is more challenging, as these stars are difficult to distinguish being dominated by the in situ disk stars, even when chemical and dynamical details are added (Ruchti et al. 2015). Nevertheless, three new prograde streams were recently discovered: Nyx (Necib et al. 2020), Aleph, and Wukong (Naidu et al. 2020).

Large unbiased (non-kinematically selected) samples of stars with accurate 6D phase-space information and chemical properties for classification and characterization can be obtained from high-precision data already (or soon to be) available.

The Gaia second Data Release (DR2; Gaia Collaboration et al. 2018) provides unprecedented accurate measurements of parallax and proper motion for more than 1.3 billion stars across the whole sky. The Apache Point Observatory Galactic Evolution Experiment sixteenth Data Release (APOGEE DR16; Majewski et al. 2017; Ahumada et al. 2020) and the Galactic Archaeology with HERMES second Data Release (GALAH DR2; De Silva et al. 2015; Buder et al. 2018) have contributed high-resolution ($R \sim 22,500$ near-infrared and $R \sim 28,000$ optical, respectively) spectra yielding precise radial velocities, stellar parameters, and abundances for more than 20 chemical elements.

Here, we exploit the excellent synergy between the aforementioned surveys, and take advantage of these high-quality data to study chemo-kinematical signatures in the local halo, with particular attention to finding and characterizing accreted material toward the disk.

2. Data and Sample Selection

This study starts with assembling a chemo-kinematical catalog by cross-matching Gaia DR2, APOGEE DR16, and GALAH DR2.

It contains Gaia positions, parallaxes, and proper motions (Lindgren et al. 2018), plus radial velocities and chemical abundances derived with the APOGEE and GALAH stellar spectra parameters pipelines (e.g., Holtzman et al. 2015; García Pérez et al. 2016; Kos et al. 2017; Buder et al. 2018). In case of multiple spectroscopic observations, we adopt the one with highest nominal signal-to-noise ratio (S/N).

First, we select objects having renormalized unit weight error (RUWE) ≤ 1.4 , as extracted from Gaia. This is to discard sources with problematic astrometric solutions, astrometric binaries, and other anomalous cases (Lindgren 2018). Next, we retain only stars with three Gaia photometric bands and relative parallax error $\varpi/\sigma_\varpi > 5$ (i.e., inverse-parallax distances better than 20%) for a total of 578,976 objects.

For the selection of sufficiently good APOGEE spectra, we reject stars with $S/N < 50$ and $\chi^2 < 25$ (Queiroz et al. 2020). As for the GALAH data, we remove stars with flags warning of poor stellar parameters, and those with $S/N < 20$, as per Hayden et al. (2020).

Therefore, we are left with a “science” sample of 437,572 stars down to $G = 18$ mag. Median uncertainties are: 0.03 mas in parallax, $\sim 50 \mu\text{as yr}^{-1}$ in proper motion, and $\sim 40 \text{ m s}^{-1}$ in line-of-sight velocity for the 247,013 Gaia-APOGEE and 190,559 Gaia-GALAH sources.

Galactic coordinates⁶ and velocity components are derived by assuming that the Sun is 8.2 kpc away from the MW center, the local standard of rest (LSR) rotates at $V_{\text{LSR}} = 232 \text{ km s}^{-1}$ around the Galactic center (McMillan 2010), and the LSR peculiar velocity of the Sun is $(U, V, W)_\odot = (11.1, 12.24, 7.25) \text{ km s}^{-1}$ (Schönrich et al. 2010). Median uncertainties of the resulting Galactocentric velocities are below 0.5 km s^{-1} for each component.

We also compute the orbital parameters of each entry (e.g., eccentricity and Z_{max}) by adopting the Galactic potential model `MWPotential2014` from Bovy (2015).

Figure 1 shows the chemical plane, $[\text{Mg}/\text{Fe}]$ – $[\text{Fe}/\text{H}]$, for the full chemo-kinematical catalog.⁷ Clearly, the sample is dominated by thin and thick disk stars. We chemically identify halo stars by taking objects with $[\text{Fe}/\text{H}] < -1.0$ and with $[\text{Mg}/\text{Fe}]$ according to the relation

$$[\text{Mg}/\text{Fe}] < -0.2 - 0.5 \cdot ([\text{Fe}/\text{H}] + 0.2), \quad (1)$$

that we derived from Mackereth et al. (2019).

We emphasize that this selection allows us to look for the metal-poor component of accreted streams with disk-like kinematics right down the Galactic plane. Alternatively, prograde streams can be also detected using stellar samples selected *above* the plane without any metallicity cuts (e.g., $|Z| > 2 \text{ kpc}$ as in Naidu et al. 2020); however, such a methodology cannot clearly identify accreted debris with thin disk-like kinematics.

⁶ We employ right-handed frames of reference with the axes positive toward the Galactic center, in the direction of Galactic rotation, and toward the North Galactic Pole, respectively.

⁷ The contribution of APOGEE and GALAH is shown separately. Clearly, individual elemental abundances, derived with the multi-step approach “SME + The Cannon” for the GALAH spectra, are underestimated for low-metallicity objects. Nevertheless, this survey remains appropriate to select halo tracers.

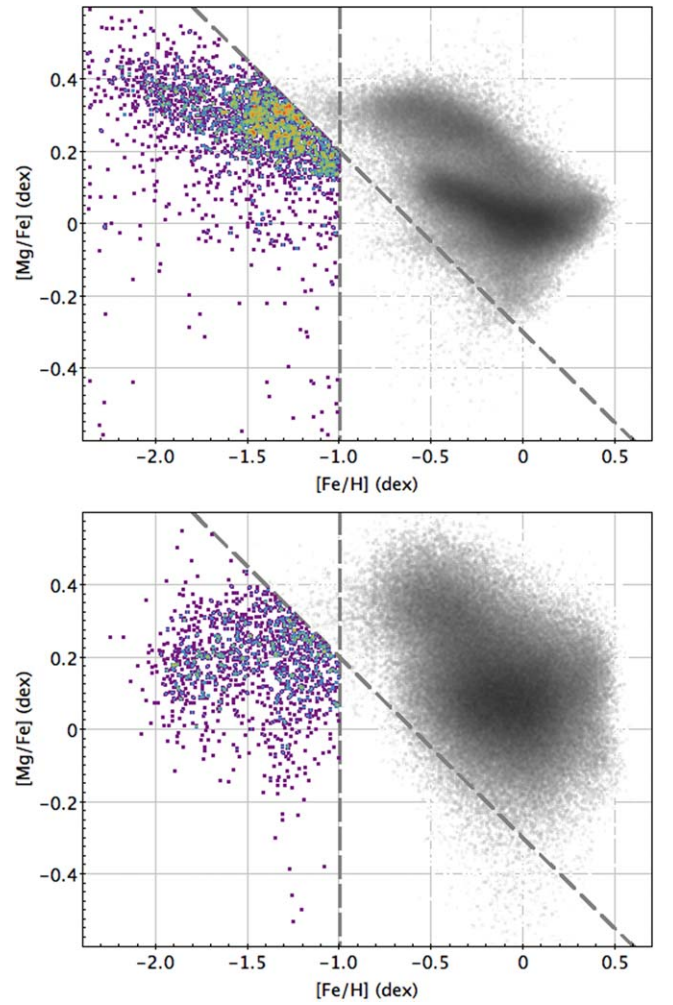


Figure 1. Top panel: chemical distribution, $[\text{Mg}/\text{Fe}]$ – $[\text{Fe}/\text{H}]$, for the 247,013 Gaia-APOGEE stars. The dashed lines represent the adopted selection of 2517 halo stars (color), separated from the thick/thin disk stars (gray). Bottom panel: same distribution as the top panel for the 1264 halo stars selected among the 190,559 Gaia-GALAH stars.

In the kinematical analysis below we further remove known members of globular clusters, dSph (e.g., Gaia Collaboration et al. 2018), visual binaries, and common proper motion pairs. This last selection leaves 3781 halo stars up to 10 kpc.

3. Results

Focusing on the sample of 1137 stars to 2.5 kpc of the Sun, we attempt detection and characterization of kinematical halo substructures in the solar vicinity as stars moving with similar space-velocities.

3.1. Stream Detection

The velocity distribution of the above sample is consistent with the superposition of stars belonging to the MW halo and metal-weak thick disk.

Following the two-point velocity correlation function methodology in Re Fiorentin et al. (2015), we quantify deviations from the smooth kinematical distribution expected for the background population, possibly due to moving groups; K -medoids cluster analysis in velocity space is then applied for final confirmation of substructures.

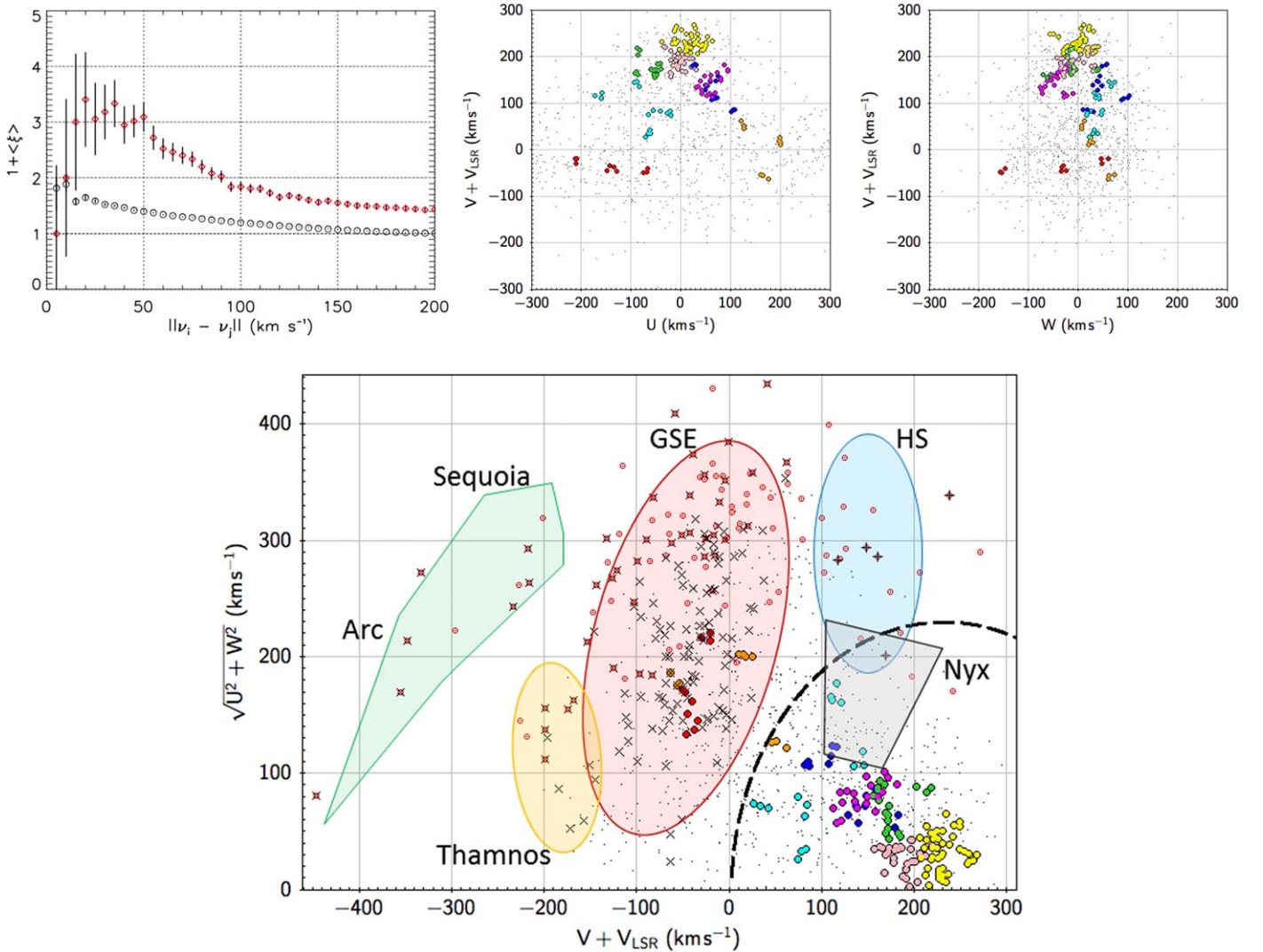


Figure 2. Top-left panel: cumulative velocity correlation function for the 1137 chemically selected nearby ($d < 2.5$ kpc) halo stars (circles), and the 10% fastest (diamonds); bins of 5 km s^{-1} width are used. The error bars are derived from Poisson’s statistics of the counts. Top-middle and top-right panels: 3D velocity distribution (detection space). Filled dots show the 163 sources with pairwise velocity differences less than 15 km s^{-1} . Different colors indicate stars associated with the eight clumps recovered by the clustering analysis. Bottom panel: Toomre diagram of the full selected sample, as above. The 10% fastest are marked with red open dots. Members of GSE (x) and Helmi Stream (HS; +) are highlighted. The approximate location of known substructures (GSE, HS, Nyx, Sequoia, the “arc,” and Thamnos) is shown. The (conservative) kinematical selection threshold for halo stars, $\|\mathbf{v} - \mathbf{v}_{\text{LSR}}\| > 230 \text{ km s}^{-1}$, is represented by the dashed line.

Figure 2 (top-left panel) shows $\xi(|\mathbf{v}_i - \mathbf{v}_j|)$ for the full sample of 1137 stars (circles), and separately for the subsample of the 10% fastest (diamonds). Clumping due to kinematical substructures (i.e., groups of particles moving coherently) is evident for values of $\langle \xi \rangle > 1$. There is a statistically significant signal for the full sample that peaks at $10\text{--}15 \text{ km s}^{-1}$; it appears even stronger for the fastest subset.

Next, we concentrate on the 163 stars with velocity differences less than 15 km s^{-1} ; this number excludes stars generating isolated velocity-pairs to make the analysis more robust.

We assign membership to these objects by using the implementation of the K -medoids clustering in 3D (U, V, W) velocity space (see e.g., Hastie et al. 2001) developed as part of the *R Project for Statistical Computing*: www.r-project.org.

In order to get final identification, we compare runs with different K -classes and we choose the solution with the best Jaccard’s index, J , that is an indicator of the stability of the groups (Tan et al. 2018).

Gauging the similarity of the K -classes obtained for 100 randomly selected half-samples, we find that $K = 8$ maximizes J for all the detected clusters (Table 1).

In Figure 2 we show in detection space these eight kinematical streams that, among the full sample, are visualized as filled dots with different colors (top-middle and top-right panels); we also present the Toomre diagram (bottom panel). Here, the 10% fastest objects are highlighted with red open dots, stars classified as GSE members by Helmi et al. (2018) are marked with a times sign, and Helmi Stream (HS) members, as found in Koppelman et al. (2019a), with a plus sign. We also show the approximate location⁸ of known substructures (e.g., GSE, HS, Nyx, Sequoia, and Thamnos), which encompass the bulk of the high-velocity stars and new GSE members from our two retrograde groups.

⁸ The regions shown are based on Figure 2 in Koppelman et al. (2019b) as well as on known members of HS, GSE, and Nyx listed in Koppelman et al. (2019a), Helmi et al. (2018), and Necib et al. (2020), respectively.

Table 1
Chemo-dynamical Mean Characteristics of the Eight Kinematical Groups

Group	N.	J	$\langle[\text{Fe}/\text{H}]\rangle$		$\langle[\text{Mg}/\text{Fe}]\rangle$		$\langle U \rangle$		$\langle V + V_{\text{LSR}} \rangle$		$\langle W \rangle$		$\langle L_z \rangle$		$\langle L_{xy} \rangle$		$\langle Z_{\text{max}} \rangle$		$\langle e \rangle$	
			(dex)		(dex)		(km s^{-1})		(km s^{-1})		(km s^{-1})		(kpc km s^{-1})		(kpc km s^{-1})		(kpc)		μ	σ
			μ	σ	μ	σ	μ	σ	μ	σ	μ	σ	μ	σ	μ	σ	μ	σ	μ	σ
1-orange	10	0.86	-1.36	0.22	0.22	0.06	168	31	5	44	32	23	-7	379	268	132	1.77	0.93	0.87	0.09
2-cyan	17	0.79	-1.50	0.28	0.20	0.16	-82	49	88	37	40	16	783	333	377	166	1.78	0.87	0.68	0.14
3-pink	29	0.74	-1.37	0.28	0.14	0.18	-3	16	187	16	-7	25	1474	148	219	100	0.66	0.47	0.23	0.07
4-yellow ^a	44	0.85	-1.45	0.37	-0.02	0.25	18	22	231	16	1	21	1875	166	153	140	0.48	0.59	0.11	0.05
5-blue	16	0.81	-1.50	0.37	0.20	0.14	64	25	131	33	53	28	1052	288	457	230	1.81	1.23	0.48	0.16
6-green	18	0.82	-1.43	0.33	0.19	0.15	-62	18	176	18	-13	30	1425	142	268	144	1.01	0.63	0.33	0.06
7-magenta	19	0.94	-1.56	0.38	0.21	0.19	61	19	144	20	-45	19	1174	150	375	167	1.49	0.91	0.44	0.09
8-red	10	0.83	-1.37	0.19	0.21	0.08	-139	55	-37	10	-42	80	-285	92	548	398	3.55	2.52	0.76	0.18

Note.

^a This group is named ‘‘Icarus’’ in this article.

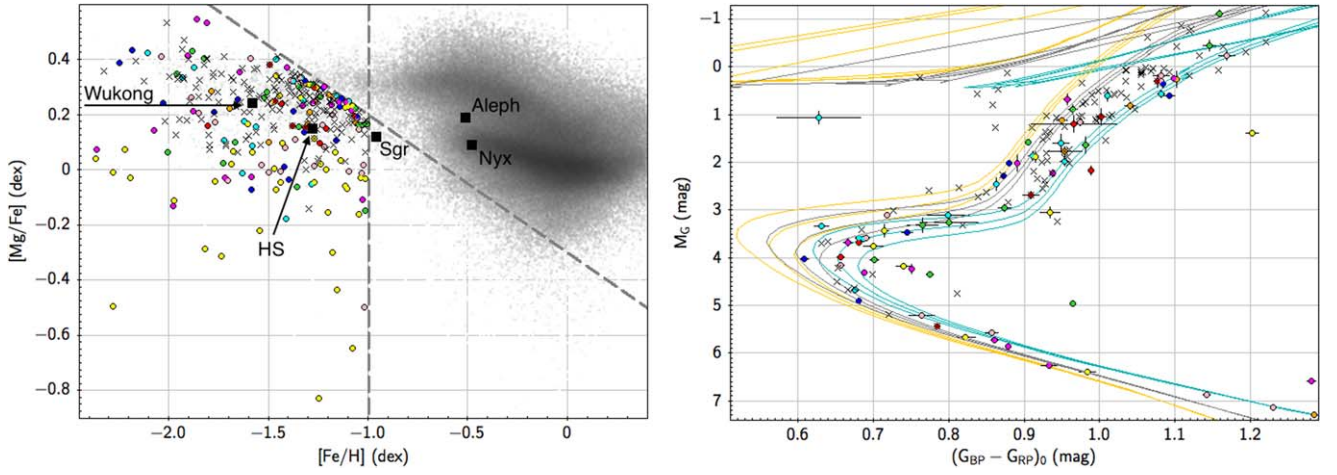


Figure 3. Distribution of the eight kinematical streams and GSE members as shown in Figure 2. Left panel: chemical abundances, $[Mg/Fe]$ – $[Fe/H]$. In the background, all of the stars in our data set. Published values for the prograde structures Nyx, Aleph, Wukong, HS, and Sagittarius (Sgr) are highlighted with squares (Necib et al. 2020; Naidu et al. 2020). Right panel: color–magnitude diagram (CMD) M_G vs. $(G_{BP} - G_{RP})_0$. We only show the stars with $|b| > 30^\circ$. Isochrones of ages 10, 12, and 14 Gyr for $[M/H] = -1.0$ (aqua), $[M/H] = -1.5$ (silver), and $[M/H] = -2.0$ (gold) are from Maíz Apellániz & Weiler (2018).

Instead, the six new prograde streams clearly belong to the region usually associated with the Galactic disk, $||v - v_{LSR}|| < 230 \text{ km s}^{-1}$.

3.2. Chemo-dynamical Properties

Table 1 lists mean values and dispersions of $[Fe/H]$, $[Mg/Fe]$, (U, V, W) , (L_z, L_{xy}) , Z_{max} , and eccentricity e . Also, Figure 3 (left panel) shows the distribution $[Mg/Fe]$ – $[Fe/H]$ for the full chemo-kinematical catalog, the members of the eight groups, and the GSE objects. The loci of the prograde structures Nyx, Aleph, Wukong, HS, and Sagittarius are marked with their published values (squares).

Group 1 (orange filled dots) and Group 8 (red) are slightly retrograde substructures, which appear associated with GSE: they have high eccentricity ($\langle e \rangle \gtrsim 0.7$) and Z_{max} (up to 7 kpc), confirming that such debris are part of the accreted halo.

Among our six prograde substructures, the most noticeable is Group 4 (yellow). It is a circular structure ($\langle e \rangle \lesssim 0.11$) confined to move close to the Galactic plane ($\langle Z_{max} \rangle \lesssim 0.5 \text{ kpc}$) with typical thin disk kinematics ($\langle V + V_{LSR} \rangle \simeq 231 \text{ km s}^{-1}$ and $\sigma_V \simeq 16 \text{ km s}^{-1}$). However, its chemical composition is not consistent with the abundances expected for the native MW thin disk. The low-metallicity, $\langle [Fe/H] \rangle \simeq -1.4$, and low α -abundance, $\langle [Mg/Fe] \rangle \simeq 0$ of Group 4 indicate that these stars are most likely debris from an accreted satellite. To the best of our knowledge, this is the first detection of a flat prograde fast-rotating stream in the MW disk. Because of its characteristics, we name Group 4 “Icarus.”⁹

Group 3 (pink) and Group 6 (green) are characterized by quite flat and circular orbits with $\langle Z_{max} \rangle \lesssim 1 \text{ kpc}$ and $\langle e \rangle \lesssim 0.3$. Despite a rotation velocity that is similar to the thick disk, $\langle V + V_{LSR} \rangle \sim 180 \text{ km s}^{-1}$, these groups are significantly more metal-poor ($\langle [Fe/H] \rangle \simeq -1.4$); furthermore, they show intermediate α -abundances ($\langle [Mg/Fe] \rangle \lesssim +0.2$) that are not consistent even with the α -enhanced metal-weak tail of the thick disk (Naidu et al. 2020). Such chemo-dynamical

properties confirm that these groups must be debris of past merging events.

An accreted origin is also expected for Group 5 (blue) and Group 7 (magenta), which show chemical compositions similar to Group 3 and 6 ($\langle [Fe/H] \rangle \simeq -1.5$ and $\langle [Mg/Fe] \rangle \simeq +0.2$). We argue that they are debris from two passages of the same satellite, as their mean angular momentum and eccentricity are quite similar, while the vertical velocity components are close in modulus but opposite directions: $\langle W \rangle = +53 \text{ km s}^{-1}$ and -45 km s^{-1} for Group 5 and Group 7, respectively.

Finally, Group 2 (cyan) is a halo stream with mean velocity $(\langle U \rangle, \langle V + V_{LSR} \rangle, \langle W \rangle) \simeq (-82, 88, 40) \text{ km s}^{-1}$ and high-eccentricity $\langle e \rangle \simeq 0.68$. Its chemical composition similar to Groups 5, 6, and 7 ($\langle [Fe/H] \rangle \simeq -1.5$ and $\langle [Mg/Fe] \rangle \simeq +0.20$) confirms that it belongs to the accreted component of the MW halo.

3.3. Hints on the Age

Figure 3 (right panel) shows members of the eight kinematical streams and GSE in the color–magnitude diagram (CMD) M_G versus $(G_{BP} - G_{RP})_0$. All of the stars have been corrected for extinction using the maps of Schlafly & Finkbeiner (2011). Only objects with $(G_{BP} - G_{RP})_0 < 1.3$ and $|b| > 30^\circ$ are shown. Error bars include parallax and photometric errors, as well as extinction uncertainties. For reference, PARSEC-COLIBRI (Bressan et al. 2012; Marigo et al. 2017) isochrones¹⁰ with stellar age 10, 12, and 14 Gyr and metallicities $[M/H] = -1.0$ (aqua), $[M/H] = -1.5$ (silver), and $[M/H] = -2.0$ (gold) are also shown.

A closer look at Figure 3 (right panel) reveals some intriguing features. The color of the RGB stars shows significant dispersion, corroborating the spectroscopic evidence of a metallicity spread. The bulk of RGB stars seems to be well constrained by our isochrones with $[M/H] = -1.0$ and -1.5 . In terms of age, stars in both our streams and GSE appear to be described by an old population. Indeed, if a metallicity $[M/H] = -1.0$ is adopted, the age range is between 10 and 13 Gyr, whereas it is closer to 13 Gyr if one adopts metal poorer isochrones. We point out that a non-negligible fraction

⁹ In Greek mythology, Icarus is the son of Daedalus. He ignored his father’s advice not to fly too close to the Sun and fell into the sea. Similarly, our Icarus stream appears to be originated from a dwarf galaxy that traveled too close to the MW; its debris are now fully spread in the “ocean” of disk stars and seen to be flat and fast-rotating with the Sun.

¹⁰ Transmission curves are from Maíz Apellániz & Weiler (2018).

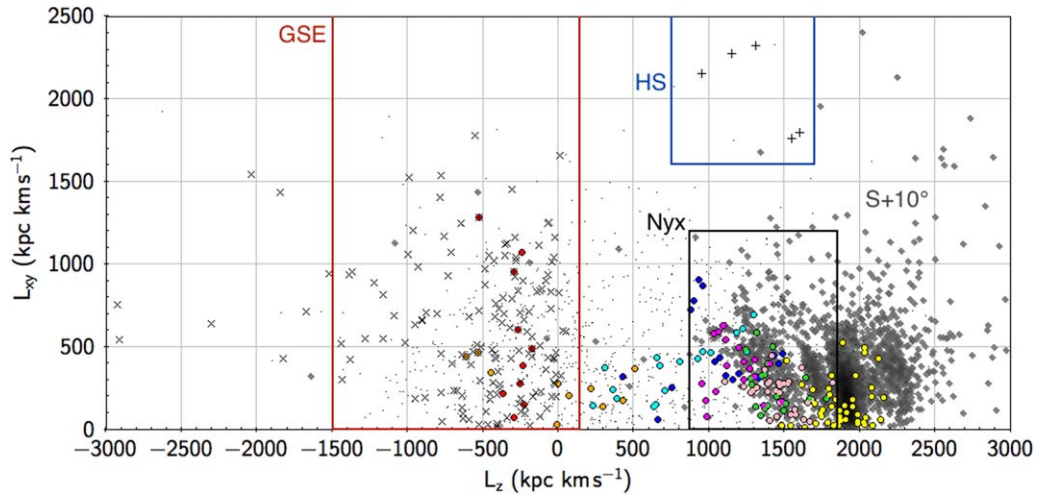


Figure 4. Space of adiabatic invariants, L_{xy} - L_z , for all the objects shown in Figure 2, including the eight streams, GSE and HS members. Solid boxes show the location of GSE, HS, and Nyx. The debris of the simulated 10° -inclination prograde satellite analyzed in Re Fiorentin et al. (2015) are overplotted for comparison (diamonds).

of the stars is redder than our most metal-rich isochrones (with the exception of the star with $(G_{BP} - G_{RP})_0 \approx 0.63$ and $M_G \approx 1$, which shows evidence of variability). These less extreme outliers may be due to unresolved binaries, enhancement in α -elements (the PARSEC-COLIBRI isochrones have solar-scaled composition), underestimated chemical composition errors, or lower accuracy of extinction estimates.

3.4. Comparison to Simulations

The analysis above has revealed two substructures associated with GSE and six new prograde streams. Their stars are old and their chemo-dynamical properties are clearly evidence of ancient mergers.

In order to better characterize the six co-rotating substructures, we compare our results to high-resolution N -body numerical simulations of minor¹¹ mergers published by Murante et al. (2010) and used to study galaxy interactions and properties of accreted debris around the Sun by Re Fiorentin et al. (2015).

We explore the space of “integrals of motion” defined by the components of angular momentum in and out the Galaxy’s disk. Figure 4 shows the plane L_{xy} - L_z for the full sample of 1137 metal-poor stars chemically selected by means of Equation (1) (dots); stars associated with the eight lumps recovered by our cluster analysis in velocity space, as well as GSE and HS members, are visualized as before. Solid boxes show the loci of GSE, HS, and Nyx. The 3585 simulated stars from the 10° -inclination prograde satellite ($S+10^\circ$), selected within a sphere of 2.5 kpc centered at the “Sun,” are overplotted (diamonds).

The consistency between the simulation and the prograde substructures is remarkable. In particular, Figure 4 indicates that Icarus represents the debris of a low-inclination prograde satellite with a stellar mass $\sim 10^9 M_\odot$, similar to the LMC. In fact, a massive satellite on a 10° -inclination prograde orbit, because of the efficient action of dynamical friction, quickly loses its orbital energy and circularize. Thus, it proceeds to the inner regions of the main halo, and leaves debris, stripped

during multiple passages, with disk-like kinematics (see Figures 6–7 in Re Fiorentin et al. 2015, yellow dots).

Groups 3, 5, 6, and 7 might be either streams produced by previous orbital passages of the same progenitor of Icarus, or remnants from different satellites accreted along an initial prograde orbit with inclination $> +10^\circ$. It is also plausible that these groups belong to Nyx and include its low-energy members; such accreted objects are more difficult to be separated from the in situ stars and could not be efficiently detected by the classification algorithm of Necib et al. (2020).

Finally, the nature of Group 2 remains uncertain, as it does not appear to be associated with either Icarus, HS, or Nyx; it might represent the prograde tail of GSE. However, its progenitor should be a satellite on an intermediate-inclination, prograde, or slightly retrograde, orbit.

4. Discussion and Conclusions

We have assembled a chemo-kinematical catalog based on top-quality astrometric and spectroscopic data from Gaia DR2, APOGEE DR16, and GALAH DR2. This data set can be exploited to explore a spherical volume around the Sun up to 10 kpc.

We have chemically selected a sample of 1137 stars to 2.5 kpc, and carried out statistical analysis and classification of their kinematics. Members of known substructures (e.g., HS, GSE, Sequoia, and Thamnos, by Helmi et al. 1999, Belokurov et al. 2018, Helmi et al. 2018, Myeong et al. 2019, and Koppelman et al. 2019b, respectively) are present in the 10% fastest subsample.

Among the subsample of 163 objects with relative velocity less than 15 km s^{-1} , we have found statistical evidence of eight kinematical substructures. The low α -abundances of their members is quite consistent with the low-metallicity tail of a progenitor dwarf galaxy similar to the LMC (Nidever et al. 2020). Also, comparing their CMD to PARSEC-COLIBRI isochrones, these substructures appear to be older than 10 Gyr.

The two retrograde groups are associated with GSE, while the six prograde substructures are located in a region that was difficult to explore with the halo sample selection criteria traditionally applied. We have further investigated their origin by means of comparison to high-resolution N -body numerical

¹¹ $M_{\text{primary}}/M_{\text{satellite}} \sim 40$, similar to the estimated mass ratio of the MW relative to the Large Magellanic Cloud (LMC).

simulations of the interaction between a MW-like galaxy and orbiting LMC-like dwarf galaxies (Murante et al. 2010).

Most noticeable, the new Group 4, that we named Icarus, is the “flattest” among the fast-rotating streams previously found in the Galactic disk. Clearly, the stellar ages greater than 10 Gyr rule out the possibility that this kinematical group is formed by in situ disk stars. Instead, its peculiar chemo-dynamical properties ($\langle[\text{Fe}/\text{H}]\rangle \simeq -1.45$, $\langle[\text{Mg}/\text{Fe}]\rangle \simeq -0.02$, and $\langle e \rangle \simeq 0.11$) are consistent with debris from a dwarf galaxy progenitor with a stellar mass of $\sim 10^9 M_\odot$ on an initial prograde very low-inclination orbit. We notice that it shares dynamical properties similar to Aleph, the metal-rich stream ($\langle[\text{Fe}/\text{H}]\rangle \simeq -0.5$), discovered outside the plane ($|Z| > 2$ kpc) by Naidu et al. (2020) and extending up to 10 kpc.

It is plausible that Groups 3, 5, 6, 7 are either streams previously released by the same progenitor of Icarus, or remnants from different satellites accreted along an initial prograde orbit, but with inclinations $> +10^\circ$. These debris could also be low-energy members of Nyx (Necib et al. 2020).





As for Group 2, the high eccentricity and low angular momentum ($\langle e \rangle \simeq 0.7$, $\langle L_{xy} \rangle \simeq 377$ kpc km s $^{-1}$) exclude its association with any of Icarus, HS, and Nyx. It is chemically similar to Wukong (Naidu et al. 2020) and GSE; if they could have a common origin, Group 2 would represent debris from a more recent passage of the Wukong progenitor or the prograde tail of GSE.

Future work will have to disentangle on the common origin of these streams, based on even better data from the next releases of Gaia and in continuous synergy with ground-based spectroscopic surveys.

We are grateful to the anonymous referee for comments that helped us improve the original manuscript. We wish to thank A. Curir, E. Poggio, and R.L. Smart for helpful discussions. M.C. acknowledges the support of INFN “Iniziativa specifica TASP.” We are indebted to the Italian Space Agency (ASI) for their continuing support through contract 2018-24-HH.0 to the National Institute for Astrophysics (INAF). This work has made use of data from the European Space Agency (ESA) mission Gaia (<https://www.cosmos.esa.int/gaia>), processed by the Gaia Data Processing and Analysis Consortium (DPAC, <https://www.cosmos.esa.int/web/gaia/dpac/consortium>). Funding for the DPAC has been provided by national institutions, in particular the institutions participating in the Gaia Multilateral Agreement. Funding for the Sloan Digital Sky Survey IV has been provided by the Alfred P. Sloan Foundation, the U.S. Department of Energy Office of Science, and the Participating Institutions. SDSS-IV acknowledges support and resources from the Center for High Performance Computing at the University of Utah. The SDSS website is www.sdss.org. SDSS-IV is managed by the Astrophysical Research Consortium for the Participating Institutions of the SDSS Collaboration including the Brazilian Participation Group, the Carnegie Institution for Science, Carnegie Mellon University, Center for Astrophysics | Harvard & Smithsonian, the Chilean Participation Group, the French Participation Group, Instituto de Astrofísica de Canarias, The Johns Hopkins University, Kavli Institute for the Physics and Mathematics of the Universe (IPMU)/University of Tokyo, the Korean Participation Group, Lawrence Berkeley National Laboratory, Leibniz Institut für Astrophysik Potsdam (AIP), Max-Planck-Institut für Astronomie (MPIA Heidelberg), Max-Planck-Institut für Astrophysik (MPA Garching), Max-Planck-Institut für Extraterrestrische Physik

(MPE), National Astronomical Observatories of China, New Mexico State University, New York University, University of Notre Dame, Observatório Nacional/MCTI, The Ohio State University, Pennsylvania State University, Shanghai Astronomical Observatory, United Kingdom Participation Group, Universidad Nacional Autónoma de México, University of Arizona, University of Colorado Boulder, University of Oxford, University of Portsmouth, University of Utah, University of Virginia, University of Washington, University of Wisconsin, Vanderbilt University, and Yale University. Based on data acquired through the Australian Astronomical Observatory, under programmes: A/2013B/13 (The GALAH pilot survey); A/2014A/25, A/2015A/19, A2017A/18 (The GALAH survey).

ORCID iDs

Paola Re Fiorentin  <https://orcid.org/0000-0002-4995-0475>
 Alessandro Spagna  <https://orcid.org/0000-0003-1732-2412>
 Mario G. Lattanzi  <https://orcid.org/0000-0003-0429-7748>
 Michele Cignoni  <https://orcid.org/0000-0001-6291-6813>

References

- Ahumada, R., Allende Prieto, C., Almeida, A., et al. 2020, *ApJS*, 249, 3
 Belokurov, V., Erkal, D., Evans, N. W., Koposov, S. E., & Deason, A. J. 2018, *MNRAS*, 478, 611
 Bovy, J. 2015, *ApJS*, 216, 29
 Bressan, A., Marigo, P., Girardi, L., et al. 2012, *MNRAS*, 427, 127
 Buder, S., Asplund, M., Duong, L., et al. 2018, *MNRAS*, 478, 4513
 Bullock, J. S., & Johnston, K. V. 2005, *ApJ*, 635, 931
 Cooper, A. P., Cole, S., Frenk, C. S., et al. 2010, *MNRAS*, 406, 744
 De Silva, G. M., Freeman, K. C., Bland-Hawthorn, J., et al. 2015, *MNRAS*, 449, 2604
 Di Matteo, P., Haywood, M., Lehnert, M. D., et al. 2019, *A&A*, 632, A4
 Fattahi, A., Deason, A. J., Frenk, C. S., et al. 2020, *MNRAS*, 497, 4459
 Gaia Collaboration, Brown, A. G. A., Vallenari, A., et al. 2018, *A&A*, 616, A1
 Gaia Collaboration, Helmi, A., van Leeuwen, F., et al. 2018, *A&A*, 616, A12
 Gallart, C., Bernard, E. J., Brook, C. B., et al. 2019, *NatAs*, 3, 932
 García Pérez, A. E., Allende Prieto, C., Holtzman, J. A., et al. 2016, *AJ*, 151, 144
 Hastie, T., Tibshirani, R., & Friedman, J. 2001, *The Elements of Statistical Learning* (Berlin: Springer)
 Hayden, M. R., Bland-Hawthorn, J., Sharma, S., et al. 2020, *MNRAS*, 493, 2952
 Helmi, A., Babusiaux, C., Koppelman, H. H., et al. 2018, *Natur*, 563, 85
 Helmi, A., White, S. D. M., de Zeeuw, P. T., & Zhao, H. 1999, *Natur*, 402, 53
 Holtzman, J. A., Schetrone, M., Johnson, J. A., et al. 2015, *AJ*, 150, 148
 Ibata, R. A., Gilmore, G., & Irwin, M. J. 1994, *Natur*, 370, 194
 Johnston, K. V. 1998, *ApJ*, 495, 297
 Klement, R. J. 2010, *A&AR*, 18, 567
 Koppelman, H. H., Helmi, A., Massari, D., Price-Whelan, A. M., & Starkenburg, T. K. 2019b, *A&A*, 631, L9
 Koppelman, H. H., Helmi, A., Massari, D., Roelenga, S., & Bastian, U. 2019a, *A&A*, 625, A5
 Kos, J., Lin, J., Zwitter, T., et al. 2017, *MNRAS*, 464, 1259
 Lindegren, L. 2018, Tech. rep., GAIA-C3-TN-LU-LL-124, http://www.rssd.esa.int/doc_fetch.php?id=3757412
 Lindegren, L., Hernandez, J., Bombrun, A., et al. 2018, *A&A*, 616, A2
 Mackereth, J. T., Schiavon, R. P., Pfeffer, J., et al. 2019, *MNRAS*, 482, 3426
 Maíz Apellániz, J., & Weiler, M. 2018, *A&A*, 619, A180
 Majewski, S. R., Schiavon, R. P., Frinchaboy, P. M., et al. 2017, *AJ*, 154, 94
 Malhan, K., Ibata, R. A., & Martin, N. F. 2018, *MNRAS*, 481, 3442
 Marigo, P., Girardi, L., Bressan, A., et al. 2017, *ApJ*, 835, 77
 McMillan, P. J. 2010, *MNRAS*, 465, 76
 Murante, G., Poggio, E., Curir, A., & Villalobos, A. 2010, *ApJL*, 716, L115
 Myeong, G. C., Vasiliev, E., Iorio, G., Evans, N. W., & Belokurov, V. 2019, *MNRAS*, 488, 1235
 Naidu, R. P., Conroy, C., Bonaca, A., et al. 2020, *ApJ*, 901, 48
 Necib, L., Ostdiek, B., Lisanti, M., et al. 2020, *NatAs*, 4, 1078
 Nidever, D. L., Hasselquist, S., Hayes, C. R., et al. 2020, *ApJ*, 895, 88
 Nissen, P. E., & Schuster, W. J. 2010, *A&A*, 511, L10

Queiroz, A. B. A., Anders, F., Chiappini, C., et al. 2020, [A&A](#), **638**, [A76](#)
Re Fiorentin, P., Lattanzi, M. G., Spagna, A., & Curir, A. 2015, [AJ](#), **150**, [128](#)
Ruchti, G. R., Read, J. I., Feltzing, S., et al. 2015, [MNRAS](#), **450**, [2874](#)
Schlafly, E. F., & Finkbeiner, D. P. 2011, [ApJ](#), **737**, [103](#)
Schönrich, R., Binney, J., & Dehnen, W. 2010, [MNRAS](#), **403**, [1829](#)

Smith, M. C., Evans, N. W., Belokurov, V., et al. 2009, [MNRAS](#), **399**, [1223](#)
Tan, P. N., Steinbach, M., Karpatne, A., & Kumar, V. 2018, Introduction to Data Mining (Edinburgh: Pearson)
Yuan, Z., Myeong, G. C., Beers, T. C., et al. 2020, [ApJ](#), **891**, [39](#)